Journal of Materials Chemistry A

Accepted Manuscript

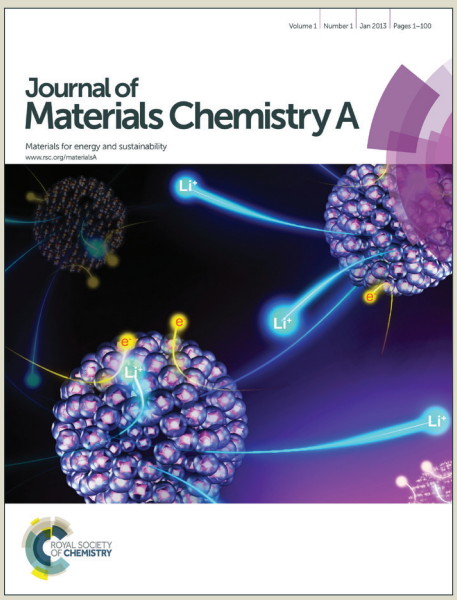

ROYAL SOCIETY OF CHEMISTRY

www.rsc.org/materialsA

Journal Name

RSCPublishing

ARTICLE

Bio-inspired Surface-functionalization of Graphene Oxide for Adsorption of Organic Dyes and Heavy Metal Ions with Superhigh Capacity

Cite this: DOI: 10.1039/x0xx00000x

Received 00th January 2012,
Accepted 00th January 2012

DOI: 10.1039/x0xx00000x

www.rsc.org/

Zhihui Dong[1,2,3], Dong Wang[1]*, Xia Liu[1], Xianfeng Pei[1], Liwei Chen[1], and Jian Jin[1]*

By ulitizling the synergistic effect of poly-dopamine (PD) with functional groups and graphene oxide (GO) with high surface area, a series of sub-nano thick PD layer coated GO (PD/GO) were fabricated by a well-controlled self-polymerization of dopamine via catechol chemistry and used for effectively decontaminated wastewater. The obtained PD/GO could selectively adsorb the dyes containing eschenmoser structure and showed extremely high adsorption capacity up to 2.1 g/g, which represents the highest value among dye adsorption reported so far. The adsorption mechanism was investigated by FTIR analysis, solution pH effect, and some control experiments. It was concluded that the adsorption process was based on eschenmoser salt assisted 1, 4-Michael addition reaction between the ortho position of catechol phenolic hydroxyl group of PD and eschenmoser group in dyes. The adsorption isotherms were explored according to Langmuir and Freundlich models, respectively. It matched well the Langmuir model. The thermodynamic parameters (ΔH, ΔG, ΔS, and E) were also calculated, which suggests an exothermic and spontaneous adsorption process. In addition, PD/GO exhibited improved adsorption capacity to heavy metal ions (53.6 mg/g for Pb^{2+}, 24.4 mg/g for Cu^{2+}, 33.3 mg/g for Cd^{2+}, and 15.2 mg/g for Hg^{2+}, respectively) than pure PD and GO. Our results indicate the effectiveness of synergistic effect of individuals on designing new functional composites with high performance.

Introduction

With the increase of progressive industrialization and urbanization, a serious environmental issue is brought in by the discharge of industrial effluents containing highly toxic organic and inorganic pollutants. The waste water discharged from the dye manufacturing, paper printing, leather, and textile industries contains many organic dye stuffs, which has a large environment, human health and economic impact. It therefore becomes an urgent issue to remove these chemical pollutants such as dyes and heavy metal ions from wastewater before they are released.[1-3] Several methods including membrane separation,[4] adsorption, filtration,[5] and ion exchange[6] were adopted to alleviate the effluent pollution. Among them, adsorption is a simple and cost-effective way. Over the years, a number of adsorbents were studied to eliminate the dyes from contaminated water, such as carbon-based nanomaterials,[7] wood waste,[8] inorganic materials,[9-12] and polymer.[13-15] Especially, carbon-based nanomaterials including active carbon,[7] graphene,[16-24] graphene oxide (GO),[25-29] and carbon nanotube[30] have been widely employed as adsorbents due to their high surface area and light weight. However, the hydrophobic surface of native carbon-based nanomaterials makes them more suitable applied in oil phase rather than in aqueous solution, thus a post-functionalization on their surfaces are usually needed. GO has been considered as one of the most promising adsorbents to be used for dyes and metal ions removal from aqueous phase. Due to the oxygen-containing groups located on GO sheet, it behaves negatively charged which can adsorb positively charged chemicals via electrostatic interaction. As a derivative of graphene, one-atom-thick GO sheets possess extremely high surface area that benefits to high adsorption capacity. Moreover, as compared to graphene, the oxygen-containing groups on GO sheet make it easier to be dispersed in water and also available for post-functionalization. Although there have been a lot of works on investigating the adsorptive property of GO,[25-29] native GO exhibited limited capacity. Effective surface functionalization of GO via a controlled and easily operated way is still highly required to achieve high capacity.[31-36]

Dopamine, a mussel-inspired protein, has recently attracted extensive interest in a broad range covering biology,[37,38] energy,[39,40] environment,[41] and nano-technology due to its super-adhesion capability on various material surfaces in the form of PD films.[42-44] Moreover, its catechol and amine groups also render dopamine an effective adsorbent for organic and inorganic chemicals. The quinones formed by catechol oxidation could react with many organic compounds under the interaction of covalent bond via Michael addition or Schiff base formation. The amine and phenolic hydroxyl groups located at

benzene ring have a strong affinity for binding metal ions. However, polydopamine suffers from serious aggregation in the form of brown particles, which is insoluble in water. It limits the utilization of the functional groups on PD, especially in base condition.[44] Obviously, as for an adsorbent, only the functional groups exposed to its outer surface play a role on adsorption capacity. Increasing the specific surface area of adsorbent is undoubtedly the effective and easy way to improve capacity.

In this work, a series of sub-nano thick PD layer coated GO (PD/GO) were fabricated by a well-controlled self-polymerization of dopamine via catechol chemistry and applied for selective dye and heavy metal ion adsorption. The designed PD/GO composite full utilizes the advantages of GO with high surface area and ultrathin PD layer with abundant functional groups exposed to outer surface. As a result, PD/GO exhibits extremely high adsorption capacity to the dyes containing eschenmoser structure up to 2.1 g/g. In comparison with reported various graphene/GO based adsorbents,[45-50] our material exhibits the highest adsorption capacity for dye adsorption and superior high adsorption capacity for heavy metal ions.

Experimental section

Synthesis of graphene oxide (GO). The GO was prepared by the modified Hummers' method.[51,52] The detail experimental procedure is described as follows: A portion of graphite flake (2 g, 100 mesh), $K_2S_2O_8$ (1 g), and P_2O_5 (1 g) were mixed with concentrated H_2SO_4 (3 ml), and then incubated at 80 °C for 6 h to peroxide the graphite. The product was dried at ambient temperature overnight after washed with distilled water and ethanol until neutral. The peroxided powder (2 g) was mixed with concentrated H_2SO_4 (50 ml) under stirring in the ice bath at 0 °C. $KMnO_4$ was added gradually to prevent the temperature exceeding 20 °C. After that, the reaction mixture was transferred to water bath in temperature of 35 °C, stirring for 2 h. Next, 92 ml water was slowly added to the mixture, and stirring was continued for 15 min. Followed by the addition of distilled water (280 ml) and treated with H_2O_2 (30%, 4 ml), the colour of the mixture turned to bright yellow. The obtained graphite oxide was centrifuged and washed with HCl (10%, 500 ml) to remove the residual metal ions. The precipitate was washed and centrifuged with distilled water repeatedly until the resulting solution becomes neutral. To exfoliate the graphite oxide, the obtained solid was treated with ultrasonic for 30 min, and centrifuged at a low-speed of 3000 rpm for 10 min to remove thick multilayer flakes, further centrifuged at 5000 rpm for 10 min to separate large flakes (precipitate) and small flakes (supernatant). The obtained precipitates were redispersed in water to get large GO suspension.

Synthesis of polydopamine coated GO (PD/GO). In detail, 5 mg GO and dopamine with mass fraction of 5%, 15%, 35%, 70%, respectively, were mixed in the Tris-HCl (pH=8.5) solution through ultrasonication. After 24 h stirring, the obtained black dispersion was centrifuged at 13000 rpm for 20 min and washed with distilled water repeatedly to remove the residual dopamine and GO without surface coating, until the supernatant was transparent. The obtained PD/GO composite was noted as PD-5%/GO, PD-15%/GO, PD-35%/GO, PD-70%/GO, respectively, corresponding to the mass fraction of dopamine.

Synthesis of polydopamine powder. 50 mg dopamine was dissolved in the Tris-HCl (pH=8.5) solution through ultrasonication. After stirred for 24 h, the black precipitate was collected by centrifuged at 13000 rpm for 20 min, followed by washed with distilled water repeatedly, until the supernatant was clear. The obtained PD solid was dried at 60 °C overnight for further use.

Dye adsorption experiment. For dye adsorption, eight typical dyes namely Methyl Orange (MO), Methylene Blue (MB), Methyl Violet (MV), Basic Fuchsin (BF), Coomassie Brilliant Blue (CBB), Rhodamine B (RHB), Malachite Green Oxalate (MGO) and Neutral Red (NR) were chosen for adsorption test. Their chemical structures were shown in Figure 1. For dye adsorption, certain amount of PD/GO solution with a known concentration was dropped into dye solution with certain concentration. The mixture was continued stirring for 5 h, and the sediment was collected and removed by centrifuge at 13000 rpm for 20 min. The concentration of residual dye solution was analyzed by UV-Vis spectroscopy by measuring the absorbance at maximum absorption wavelength. The concentration of each dye before and after adsorption was determined from the stand calibration curve.

Heavy metal ion adsorption experiment. The batch adsorption experiments of Pb (II), Cu (II), Cd (II) and Hg (II) were carried out at different pH values according to the stability of each metal ion.[41] The pH of each solution was adjusted by using 0.1 M HCl: Pb (II) in pH 4.0-5.4, Cu (II) in pH 5.2-6.8, Cd (II) in pH 5.2-6.8, and Hg (II) in pH 3.5-4.0, respectively. In a typical experiment, a certain amount of dilute PD/GO solution was added to 50 ppm metal ion solution. After stirring overnight, the precipitate was removed by centrifuge at 13000 rpm for 20 min. Inductively coupled plasma-optical emission spectroscopy (ICP-OES) was adopted to determine the residual metal ion concentration.

Characterization

AFM was measured on Agilent 5550. FTIR spectra were collected on Nicolet 6700 (Thermo Scientific). UV-Vis spectra were performed on Lambda 25 UV/Vis Spectrometer (PerkinElmer). ICP-OES results were collected on Agilent 725.

Results and discussion

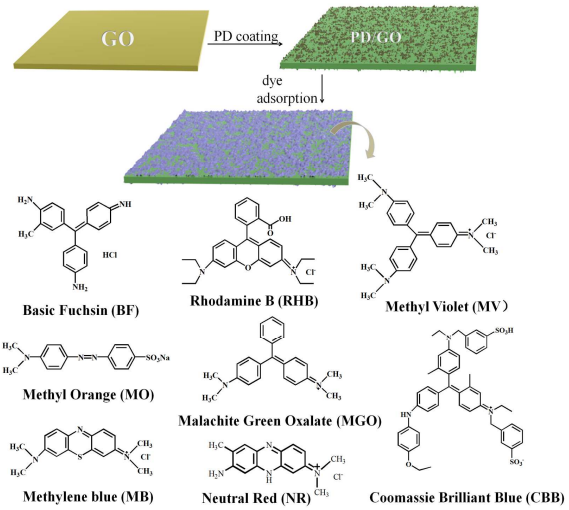

Fig. 1 Scheme for the preparation of PD/GO and the chemical structures of dyes used in this work.

The morphologies of as-prepared GO, PD-5%/GO, PD-15%/GO and PD-35%/GO were firstly examined by atomic

force microscope (AFM) as shown in Figure 2. The corresponding photographs of their suspensions were also presented in the inset of Figure 2. The thickness of GO sheet is measured to be ~1.0 nm, indicating that the GO sheets are monolayer. Due to PD coating, the thicknesses of PD-5%/GO, PD-15%/GO, and PD-35%/GO increases to be 1.3, 1.7, and 2.5 nm, respectively. All PD/GO composites could be well dispersed in aqueous solution and do not precipitate even after 2 months. PD coating on GO does not cause the aggregation of PD/GO. The thickness of PD layer could be well controlled by tuning dopamine mass fraction. With gradually increasing PD layer thickness, the colour of PD/GO dispersion becomes deeper and deeper but keeps transparent all the time. However, when the mass fraction of dopamine increases to 70%, the PD-70%/GO dispersions are not stable and precipitation form after several days. It is noted that dopamine can reduce GO partially during surface coating process.[53,54] Obviously, besides providing adsorption sites,[37-44] the existence of PD coating on GO effectively prevents the aggregation of partially reduced GO sheets.

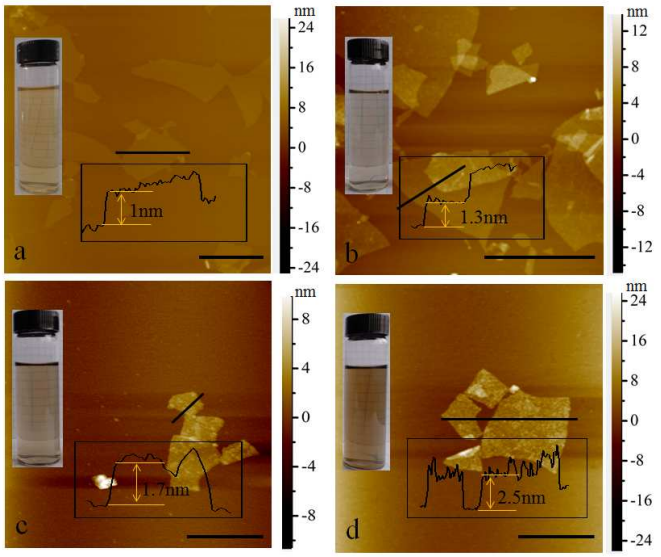

Fig. 2 AFM images of as-prepared GO (scale bar is 1 μm) and PD-5%/GO, PD-15%/GO and PD-35%/GO (scale bars are 500 nm) dropped on mica.

The adsorption performance of as-prepared GO, PD-5%/GO, PD-15%/GO, PD-35%/GO, PD-70%/GO and PD towards MB were tested. The adsorption capacity (Q_e) was calculated by using the following equation.[25-29]

$$Q_e = (C_0\text{-}C_e)V/M$$

Where C_0 is the initial concentration of MB (mg/L), C_e is the concentration of residual MB solution after maximum adsorption (mg/L), V stands for the volume of the solution (ml), and M is the mass of the adsorbent (mg). As shown in Figure 3e, PD-15%/GO exhibits the highest adsorption capacity to MB up to 1.89 g/g. This value is more than ten times higher than as-prepared GO and PD. The capacity of PD-5%/GO, PD-35%/GO, and PD-70%/G are 1.3, 1.7, 0.6 g/g, respectively. The capacity difference for PD/GO composite with different PD mass fraction is related to the synergistic effect of GO and PD. First of all, the high adsorption capacity originates from the one-atom-thick sheet structure of GO. The PD/GO composites still maintain the sheet structure well. PD coating is indeed essential for achieving high adsorption capacity. However, excess PD on GO will decrease adsorption due to only weight increase. Therefore, the ideal structure of PD/GO should be GO sheet covered by a nearly single layer of PD with molecular thickness. In addition, surface roughness is also advantageous to increase surface area, thus increase capacity. The AFM images of PD/GO composites shown in Figure 2 clearly indicate the formation of tiny PD particles, giving rise to a rather rough surface.

The PD/GO composites are characterized by SEM and Nitrogen absorption/desorption analysis (Figure 3). All PD/GO composites show clearly sheet-like structure and no obvious aggregates are observed (Figure 3a-d). The surface area of PD/GO composites based on BET data are 106 m^2/g for PD-5%/GO, 83m^2/g for PD-15%/GO, 24m^2/g for PD-35%/GO, and 12 m^2/g for PD-70%/GO, respectively (Figure 3f). The downward tendency of surface area with increasing PD content is ascribed to the mass increase of PD and little aggregation of nanosheets in case of excessive PD.

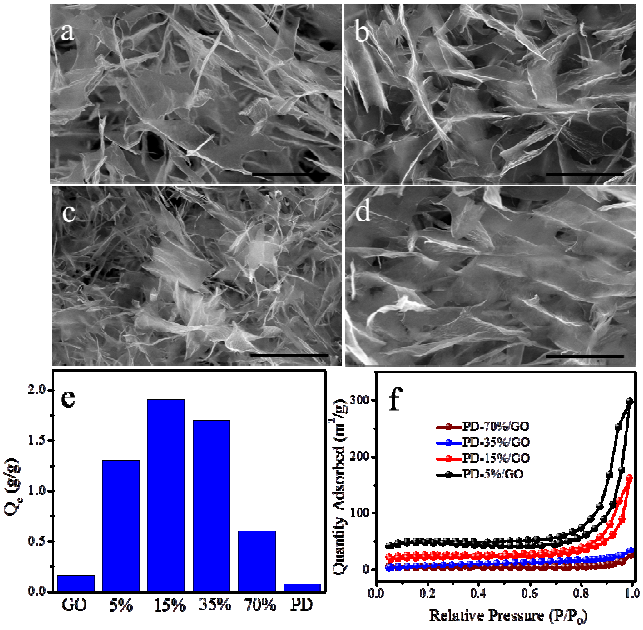

Fig. 3 (a-d) SEM images of PD-5%/GO (a), PD-15%/GO (b), PD-35%/GO (c), PD-70%/GO (d) after freeze drying (scale bars are 5μm) (e) Adsorption capacity of MB on as-prepared GO, PD-5%/GO, PD-15%/GO, PD-35%/GO, PD-70%/GO and PD. (f) Nitrogen absorption/desorption analysis of PD-5%/GO (black), PD-15%/GO (red), PD-35%/GO (blue), PD-70%/GO (brown) after freeze drying.

The adsorption of various dyes including MB, MV, MGO, CBB, BF, NR, RHB and MO on PD-15%/GO are summarized in Figure 4. PD-15%/GO exhibits extremely high adsorption capacity to the dyes containing eschenmoser structure, 1.8, 2.1, 2, 2.1, 1.7, 1.4 g/g corresponding to MB, MV, MGO, CBB, BF, NR, respectively, which are more than ten times higher than that of as-prepared GO and PD. These values are almost the highest ones reported so far and even five times higher than commercial active carbon.[7] As for other kinds of dyes, such as RHB and MGO, the capacity of PD-15%/GO is as low as 0.1, and 0.03 g/g, respectively, similar to that of as-prepared GO and PD. This result indicates that PD-15%/GO selectively adsorb eschenmoser-containing dyes.

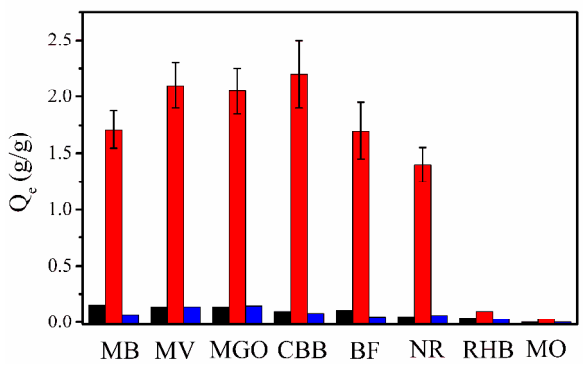

Fig. 4 Adsorption capacity of various dyes on as-prepared GO (black), PD-15%/GO (red), and PD (blue).

It is acknowledged that most of adsorbents are based on ionic interaction and host-guest interaction for dye adsorption.[55-58] As for GO, the adsorption between GO and dyes are mainly based on electrostatic attraction or weak non-covalent interaction, such as π-π interaction and van der Waals interaction as described in most of previous publications.[25-29] The adsorption process between our PD/GO and dyes are different. In order to figure out the special interaction between PD layer and eschenmoser-containing dyes, MB was used as a representative and FT-IR spectrum was adopted to analyze the interaction between PD and MB, where the specimen of PD/MB composite was obtained by mixing PD powder and MB solution. Figure 5a demonstrates the FT-IR spectra of pure PD, pure MB, and PD/MB composite. The bands at 1538, 1488, 1072, 1141, and 1245 cm^{-1} are related to skeletal vibration of the heterocycle of MB.[59] After mixed with PD, these characteristic peaks either diminish or disappear. It is ascribed to the reaction of PD and heterocycle skeleton of MB. We propose an eschenmoser salt assisted 1, 4-Michael addition reaction between the ortho position of catechol phenolic hydroxyl group of PD and eschenmoser structure of MB as drawn in Figure 5c.[60-62] If such a reaction occurs, the imide ion groups on PD/MB could react with H_3O^+ and then hydrolyze into carbonyl group. To further confirm it, PD/MB composite was treated by 0.1 M HCl. As shown in Figure 5b, a new band at 1720 cm^{-1} related to the stretching vibration of C=O appears after acid treatment. This evidence strongly supports occurrence of eschenmoser salt assisted 1, 4-Michael addition reaction between MB and PD.

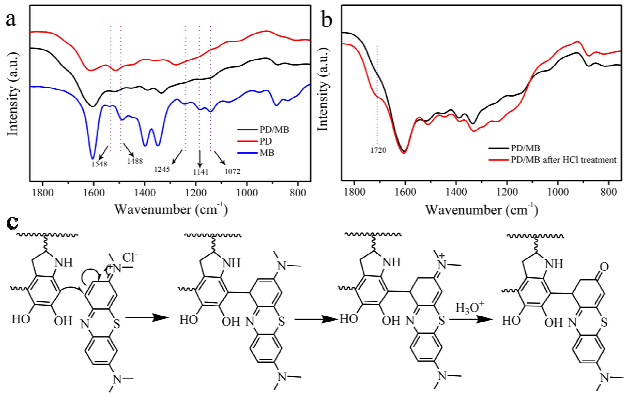

Fig. 5 (a) FT-IR spectra of as-prepared PD, MB, and PD/MB composite, respectively. (b) FT-IR spectra of PD/MB composite and PD/MB composite after treated by HCl. (c) The proposed adsorption mechanism between PD and MB.

To further confirm the adsorption mechanism between PD and MB, the effect of pH value of MB solution on adsorption property were investigated. For this purpose, PD-15%/GO was used to adsorb MB in solution with different pH (namely pH=3, 5, and 8 and the residual MB solution was tested by UV-Vis absorption spectra. As shown in Figure 6, the absorbance of the residual solution decreases with increasing pH value, corresponding to an increase of absorption capacity. This is in agreement with the adsorption mechanism based on 1,4-Michael addition where the existence of base could facilitate the adsorption reaction but acid weaken the reaction.

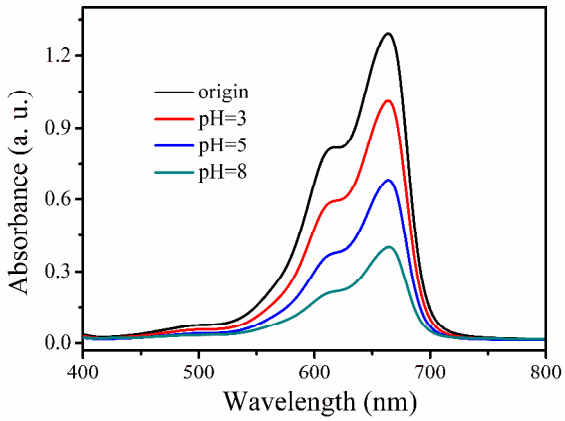

Fig. 6 UV-Vis spectra of residual MB solutions with different pH values after adsorbed by PD-15%/GO.

The adsorption thermodynamics and adsorption isotherms of PD-15%/GO were also investigated to further understand the adsorption process. The thermodynamic parameters could provide in-depth information about internal energy changes that are associated with adsorption. The UV-Vis spectra of the residual MB solutions after adsorbed by PD-15%/GO at different temperature and corresponding adsorption capacity are presented in Figure 7. The standard Gibbs free-energy change (ΔG), the standard enthalpy change (ΔH), and the standard entropy change (ΔS) of MB onto PD-15%/GO were calculated according to previous reports[25-29] and the results are listed in Figure 7c. The ΔG value is negative, suggesting the adsorption process is a spontaneous process. The negative ΔH indicates the adsorption is exothermic. It is further confirmed by the decline of adsorption capacity with the increase of temperature (Figure 7b). The negative ΔS indicate a decrease of randomness during adsorption.

The adsorption isotherm was carried on at room temperature. The adsorption capacity of MB onto PD-15%/GO against initial concentration of MB is shown in Figure 8a. It can be seen that the capacity increase with increasing the initial MB concentration. This is because that the increased driving force coming from concentration gradient accelerates the diffusion speed of MB towards PD-15%/GO. The Langmuir model and Freundlich model are used to analyze the adsorption equilibrium. The obtained related coefficients were listed in Figure 8b. According to the two coefficient R^2 values, the equilibrium data fits well Langmuir model rather than Freundlich model. It means that during the adsorption process monolayer MB cover over a homogenous surface and no subsequent interaction between adsorbents. On the basis of

Langmuir model, the maximum adsorption capacity could be 2.18 g/g, which is the highest value for MB adsorption as compared to active carbon and other adsorbents.

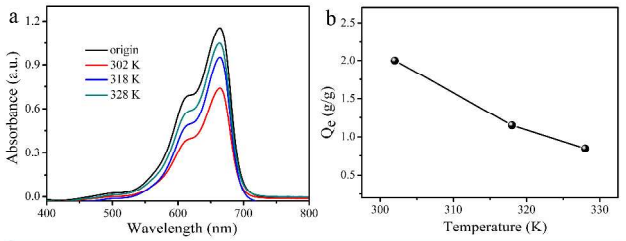

c

Thermodynamic constant	T (K) 302	318	328
Ln K	5.286	4.787	4.430
ΔG (KJ/mol)	-13.27	-12.656	-12.08
ΔH (KJ/mol)		-24.901	
ΔS (J/mol K)		-38.507	

Fig. 7 Thermodynamic analysis of adsorption process. (a) UV-Vis spectra of the residual MB solutions after adsorption at different temperature and (b) corresponding adsorption capacity. (c) Thermodynamic parameters for the adsorption of MB by PD-15%/GO.

The selective adsorption of PD/GO composites toward eschenmoser-containing dyes makes them feasible for separation of eschenmoser-containing dyes from dye mixture. To test such ability, a proof-of-concept experiment was carried out. As shown in Figure 9, two mixed solutions containing MB/RHB and MB/MO in 1:1 molar ratio were prepared in advance, respectively. Then a certain amount of PD-15%/GO was put into the two solutions to fully adsorb MB and centrifuged from the solutions. The mixed solution and residual solution were examined by UV-Vis absorption. It can be seen that after adsorption of PD-15%/GO the colours of the two mixed solutions change from deep blue and green to red and yellow, corresponding to the colour of RHB and MO (Figure 9a, b). The UV-Vis spectra clearly show that the absorption peak of MB completely disappear in the two residual solutions, indicating all MB are removed by PD-15%/GO from the mixed solutions (Figure 9c, d).

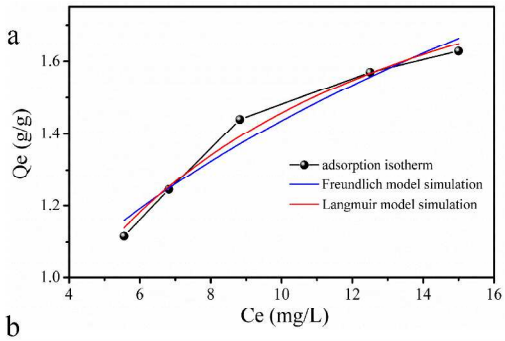

b

T (K)	Langmuir q_m(mg/g)	K_L(L/mg)	R^2	Freundlich K_F	n	R^2
302	2.181	0.2024	0.9767	0.6126	2.6737	0.9435

Fig. 8 (a) Adsorption isotherm of MB onto PD-15%/GO simulated by Langmuir model (red line) and Freundlich model (blue line). (b) Isotherm parameters for the adsorption of MB by PD-15%/GO.

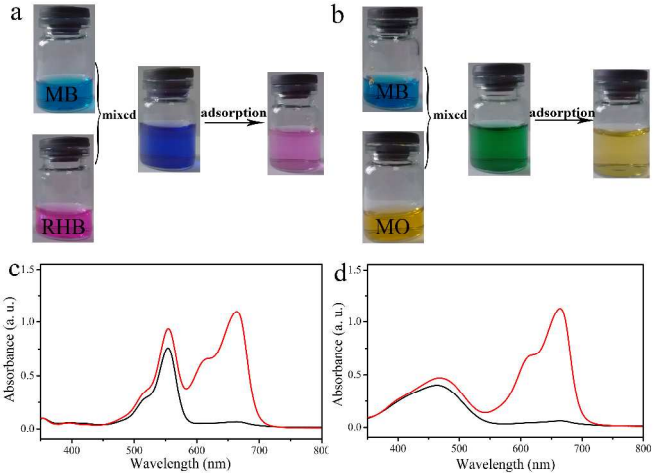

Fig. 9 Photographs of selective adsorption of MB from MB/RHB (a) and MB/MO (b) mixed solutions by using PD-15%/GO and their corresponding UV-Vis spectra before (red line) and after (black line) adsorption (c, d).

The separation efficiency (R) was calculated according to:

$$R=(1-C_m/C_0)\times 100$$

where C_m and C_0 are MB concentrations in the original MB/RHB or MB/MO mixed solution and in the solution after adsorption, respectively.[63] The calculated separation efficiency are 93.4% and 90% corresponding to MB/RHB and MB/MO mixtures, respectively.

The amine and hydroxyl groups on PD could also act as binding sites to coordinate heavy metal ions. The PD-15%/GO was therefore used to adsorb heavy metal ions. Four heavy metal ions, Pb^{2+}, Cu^{2+}, Cd^{2+}, and Hg^{2+}, which are highly toxic and well-known inorganic pollutants, are investigated. As shown in Figure 10, the capacity of Pb^{2+}, Cu^{2+}, Cd^{2+}, and Hg^{2+} are 53.6, 24.4, 33.3, and 15.2 mg/g, respectively. Correspondingly, the capacity of as-prepared GO is 22.6, 14.5, 20, and 4.35 mg/g and that of PD is 3.3, 2, 2, and 2.48 mg/g, respectively. The dramatically capacity increase of PD/GO as compared to as-prepared GO and PD demonstrates the synergetic effect of PD coating and GO nanosheet.

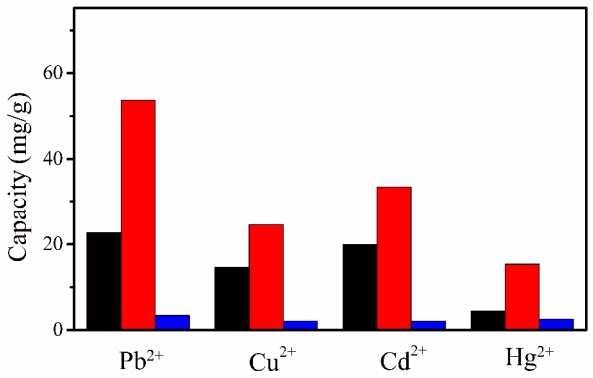

Fig. 10 Adsorption capacity of heavy metal ions on as-prepared GO (black), PD-15%/GO (red), and PD (blue).

Conclusions

In summary, we prepared PD surface-functionalized GO composite and systematically investigated the adsorptive property of dyes and heavy metal ions. A series of PD layer coated GO nanosheets with well-controlled thickness in a sub-nanometer scale could be obtained by carefully tuning the mass fraction of PD. The adsorption capacity was highly dependent on the thickness of PD coating and the pH and temperature of solution. Under the synergistic enhancement effect of PD layer and GO nanosheet, PD/GO exhibits an excellent adsorption performance especial towards eschenmoser-containing dyes. The adsorption mechanism to eschenmoser-containing dyes was explained to the chemical reaction of eschenmoser salt assisted 1, 4-Michael addition reaction. The superior adsorption capacity of the sub-nano thick PD layer coated GO makes it a promising adsorbent for decontaminating wastewater. By utilizing the synergistic reinforcement effect of polydopamine with functional multi-groups and graphene oxide with high surface area, next-generation functional nanomaterials with improved performance could be rationally designed.

Acknowledgments

This work was supported by the National Basic Research Program of China (grant no. 2013CB933000 and 2013CB933000), the National Natural Science Foundation of China (grant no. 21273270 and 21004076), the Key Development Project of Chinese Academy of Sciences (grant no KJZD-EW-M01-3), and the Natural Science Foundation of Jiangsu Province (BK20130007).

Notes and references

[1]i-LAB and Nano-Bionics Division, Suzhou Institute of Nano-Tech and Nano-Bionics, Chinese Academy of Sciences, Suzhou 215123, China, [2]Technical Institute of Physical and Chemistry, Chinese Academy of Sciences, Beijing, 100190, China, [3]University of Chinese Academy of Sciences, Chinese Academy of Sciences, Beijing, 100049, China.

Corresponding authors:
jjin2009@sinano.ac.cn; dwang2009@sinano.ac.cn

1 M. Zhang, X. Xie, M. Tang, C. S. Criddle, Y. Cui, S. X. Wang, *Nat. Comm.*, 2013, **4**, 1866.
2 I. Ali, *Chem. Rev.*, 2012, **112**, 5073.
3 M. Khajeh, S. Laurent, K. Dastafkan, *Chem. Rev.*, 2012, **113**, 7728.
4 Y. Han, Z. Xu, C. Gao, *Adv. Funct. Mater.*, 2013, **23**, 3693.
5 M. Hu, B. Mi, *Environ. Sci. Technol.*, 2013, **47**, 3715.
6 Z. Cheng, Y. Wu, N. Wang, W. Yang, T. Xu, *Ind. Eng. Chem. Res.*, 2010, **49**, 3079.
7 B. H. Hameed, A. T. M. Din, A. L. Ahmad, *J. Hazard. Mater.*, 2007, **141**, 819.
8 J. S. Piccin, L. A. Feris, M. Cooper, M. Gutterres, *J. Chem. Eng. Data*, 2013, **58**, 873.
9 N. B. Shukla, S. Rattan, G. Madras, *Ind. Eng. Chem. Res.,* 2012, **51**, 14941.
10 G. Lian, X. Zhang, S. Zhang, D. Liu, D. Cui, Q. Wang, *Energy Environ. Sci.*, 2012, **5**, 7072.
11 C. Chen, P. Gunawan, R. Xu, *J. Mater. Chem.*, 2011, **21**, 1218.
12 Y. Zhang, Z.-A. Qiao, Y. Li, Y. Liu, Q. Huo, *J. Mater. Chem.*, 2011, **21**, 17283.
13 D. Yang, S. Sarina, H. Zhu, H. Liu, Z. Zheng, M. Xie, S. V. Smith, S. Komarneni, *Angew. Chem. Int. Ed.*, 2011, **50**, 10594.
14 Z. Yan, G. Li, L. Mu, S. Tao, *J. Mater. Chem.*, 2006, **16**, 1717.
15 X. Guo, G. T. Fei, H. Su, L. D. Zhang, *J. Mater. Chem.*, 2011, **21**, 8618.
16 H. Wang, X. Yuan, Y. Wu, H. Huang, X. Peng, G. Zeng, H. Zhong, J. Liang, M. Ren, *Adv. Colloid Interface Sci.*, 2013, **195**, 19.
17 P. Lazar, F. Karlicky, P. Jurecka, M. Kocman, E. Otyepkova, K. Safarova, M. Otyepka, *J. Am. Chem. Soc.*, 2013, **135**, 6372.
18 X. Huang, Z. Yin, S. Wu, X. Qi, Q. He, Q. Zhang, Q. Yan, F. Boey, H. Zhang, *Small*, 2011, **7**, 1876.
19 X.-L. Wu, L. Wang, C.-L. Chen, A.-W. Xu, X.-K. Wang, *J. Mater. Chem.*, 2011, **21**, 17353.
20 S. M. Maliyekkal, T. S. Sreeprasad, D. Krishnan, S. Kouser, A. K. Mishra, U. V. Waghmare, T. Pradeep, *Small*, 2013, **9**, 273.
21 J. Zhao, W. Ren, H.-M. Cheng, *J. Mater. Chem.*, 2012, **22**, 20197.
22 W. Fan, W. Gao, C. Zhang, W. W. Tjiu, J. Pan, T. Liu, *J. Mater. Chem.*, 2012, **22**, 25108.
23 Z.-Q. Zhao, X. Chen, Q. Yang, J.-H. Liu, X.-J. Huang, *Chem. Commun.*, 2012, **48**, 2180.
24 Y. Yang, Y. Xie, L. Pang, M. Li, X. Song, J. Wen, H. Zhao, *Langmuir*, 2013, **29**, 10727.
25 Y. Chen, L. Chen, H. Bai, L. Li, *J. Mater. Chem. A*, 2013, **1**, 1992.
26 Z. Geng, Y. Lin, X. Yu, Q. Shen, L. Ma, Z. Li, N. Pan, X. Wang, *J. Mater. Chem.*, 2012, **22**, 3527.
27 J. Xu, L. Wang, Y. Zhu, *Langmuir*, 2012, **28**, 8418.
28 B. Li, H. Cao, J. Yin, Y. A. Wu, J. H. Warner, *J. Mater. Chem.*, 2012, **22**, 1876.
29 P. Sharma, M. R. Das, *J. Chem. Eng. Data*, 2013, **58**, 151.
30 Y. Yan, M. Zhang, K. Gong, L. Su, Z. Guo, L. Mao, *Chem. Mater.*, 2005, **17**, 3457.
31 C. J. Madadrang, H. Y. Kim, G. Gao, N. Wang, J. Zhu, H. Feng, M. Gorring, M. L. Kasner, S. Hou, *ACS Appl. Mater. Interfaces*, 2012, **4**, 1186.
32 H. Chang, H. Wu, *Energy Environ. Sci.*, 2013, **6**, 3483.
33 Y. Yuan, G. Zhang, Y. Li, G. Zhang, F. Zhang, X. Fan, *Polym. Chem.*, 2013, **4**, 2164.
34 Y. Sun, D. Shao, C. Chen, S. Yang, X. Wang, *Environ. Sci. Technol*, 2013, **47**, 9904.
35 H. Bai, K. Sheng, P. Zhang, C. Li, G. Shi, *J. Mater. Chem.*, 2011, **21**, 18653.
36 S. Zhang, M. Zeng, W. Xu, J. Li, J. Li, J. Xu, X. Wang, *Dalton Trans.*, 2013, **42**, 7854.
37 H. O. Ham, Z. Liu, K. H. Aaron Lau, H. Lee, P. B. Messersmith, *Angew. Chem. Int. Ed.*, 2011, **50**, 732.
38 J. Su, F. Chen, V. L. Cryns, P. B. Messersmith, *J. Am. Chem. Soc.*, 2011, **133**, 11850.
39 L. Wang, D. Wang, Z. Dong, F. Zhang, J. Jin, *Nano Lett.*, 2013, **13**, 1711.
40 L. Wang, D. Wang, F. Zhang, J. Jin, *Nano Lett.*, 2013, **13**, 4206.
41 M. Lee, J. Rho, D.-F. Lee, S. Hong, S.-J. Choi, P. B. Messersmith, H. Lee, *ChemPlusChem*, 2012, **77**, 987.
42. W. Lee, J. U. Lee, B. M. Jung, J.-H. Byun, J.-W. Yi, S.-B. Lee, B.-S. Kim, *Carbon*, 2013, **65**, 296.
43 L. Q. Xu, W. J. Yang, K.-G. Neoh, E.-T. Kang, G. D. Fu, *Macromolecules*, 2010, **43**, 8336.

44 H. Lee, B. P. Lee, P. B. Messersmith, *Nat.*, 2007, **448**, 338.
45 H. Jabeen, V. Chandra, S. Jung, J. W. Lee, K. S. Kim, S. B. Kim, *Nanoscale*, 2011, **3**, 3583.
46 V. Chandra, J. Park, Y. Chun, J. W. Lee, I.-C. Hwang, K. S. Kim, *ACS Nano*, 2010, **4**, 3979.
47 S. Wang, H. Sun, H. M. Ang, M. O. Tade, *Chem. Eng. J*, 2013, **226**, 336.
48 V. Chandra, K. S. Kim, *Chem. Commun.*, 2011, **47**, 3942.
49 A. Y. Romanchuk, A. S. Slesarev, S. N. Kalmykov, D. V. Kosynkin, J. M. Tour, *Phys. Chem. Chem. Phys.*, 2013, **15**, 2321.
50 Y. Wang, S. Liang, B. Chen, F. Guo, S. Yu, Y. Tang, *Plos One*, 2013, **8**, e65634.
51 W. S. Hummers, J. R. E. Offeman, *J. Am. Chem. Soc.*, 1958, **80**, 1339.
52 J. Zhao, S. Pei, W. Ren, L. Gao, H.-M. Cheng, *ACS Nano*, 2010, **9**, 5245.
53 L. Q. Xu, W. J. Yang, K.-G. Neoh, E.-T. Kang, G. D. Fu, *Macromolecules*, 2010, **43**, 8336.
54 S. M. Kang, S. Park, D. Kim, S. Y. Park, R. S. Ruoff, *Adv. Funct. Mater.*, 2011, **21**, 108.
55 M. A. Lazar, W. A. Daoud, *RSC Advances*, 2012, **2**, 447.
56 S. Xie, B. Zheng, Q. Kuang, X. Wang, Z. Xie, L. Zheng, *CrystEngComm*, 2012, **14**, 7715.
57 F. Zhang, Z. Zhao, R. Tan, Y. Guo, L. Cao, L. Chen, J. Li, W. Xu, Y. Yang, W. Song, *J. Colloid Interface Sci*, 2012, **386**, 277.
58 R. Wang, B. Yu, X. Jiang, J. Yin, *Adv. Funct. Mater.*, 2012, **22**, 2606.
59 O. V. Ovchinnikov, S. V. Chernykh, M. S. Smirnov, D. V. Alpatova, R. P. Vorobeva, A. N. Latyshev, A. B. Evlev, A. N. Utekhin, A. N. Lukin, *J. Appl. Spectrosc.*, 2007, **74**, 809.
60 H. Lee, S. M. Dellatore, W. M. Miller, P. B. Messersmith, *Science*, 2007, **318**, 426.
61 S. Hong, Y. S. Na, S. Choi, I. T. Song, W. Y. Kim, H. Lee, *Adv. Funct. Mater.*, 2012, **22**, 4711.
62 J. I. Clodt, V. Filiz, S. Rangou, K. Buhr, C. Abetz, D. Hoche, J. Hahn, A. Jung, V. Abetz, *Adv. Funct. Mater.*, 2013, **23**, 731.
63 Z. Xue, S. Wang, L. Lin, L. Chen, M. Liu, L. Feng, L. Jiang, *Adv. Mater.*, 2011, **23**, 4270.